Astron. Astrophys. 363, 269–278 (2000)

ASTRONOMY AND ASTROPHYSICS

Wavelet analysis and the determination of coronal plasma properties

I. De Moortel and A.W. Hood

School of Mathematics and Statistics, University of St Andrews, North Haugh, St Andrews, Fife KY16 9SS, Scotland

Received 7 August 2000 / Accepted 15 September 2000

Abstract. The usefulness of wavelet analysis is demonstrated by considering analytical expressions for phase mixed Alfvén waves in different physical circumstances. The wavelet analysis is briefly introduced, using the complex-valued Morlet wavelet, consisting of a plane wave modulated by a Gaussian, as the basic wavelet. The time and scale resolution of the wavelet transform are then discussed in more detail, by working out the transform of simple harmonic functions analytically. As an illustration of the power of wavelet analysis, phase mixed Alfvén waves are investigated. A comparison is made between a truly finite harmonic wave and an Alfvén wave, dissipated by phase mixing and, using the wavelet transform, it is demonstrated that it is possible to distinguish between these two 'finite' signals. It is also possible to extract the value of the dissipation coefficient from the wavelet transform. When considering phase mixing of Alfvén waves in a gravitationally stratified atmosphere, the lengthening of the wavelengths is clearly evident in the transform, which provides an independent estimate of the value of the pressure scale height. In a radially diverging atmosphere, the shortening of the wavelengths is also apparent in the wavelet transform, showing how the Alfvén speed varies along the loop and thus providing information on the coronal density and magnetic field. When applying wavelet analysis to observed wave-like oscillations, it should be possible to infer properties of the coronal plasma by making a detailed study of the wavelet transform.

Key words: Magnetohydrodynamics (MHD) – waves – Sun: activity – Sun: corona

1. Introduction

The mechanism by which the solar corona is heated is still one of the major unsolved problems in solar physics. Over the past decades, several mechanisms have been suggested (Browning 1991; Zirker 1993; Narain & Ulmschneider 1996). One possible mechanism to transfer energy from the large scale motion to small scale oscillations, i.e. to a lengthscale where dissipation can become effective, is the idea of phase mixing. Heyvaerts & Priest (1983) proposed this simple but promising idea for the behaviour of Alfvén waves when the local Alfvén speed varies across the magnetic field lines. Obviously, the detection of such oscillations in the corona is a crucial step in determining the presence and relevance of these wave heating mechanisms. Observations of periodic variations in physical quantities could indicate the presence of waves. However, as Alfvén waves do not perturb the density of the surroundings through which they propagate, they will not be observed directly as periodic intensity variations. Alfvén waves could be observed indirectly as their passage will cause line broadening. An overview of possible methods to observe MHD waves or wave heating mechanisms, using data taken by the instruments onboard of SOHO (Solar and Heliospheric Observatory) is given by Ireland (1996). Recent observations of the solar corona have clearly demonstrated the existence of wave-like motions. For example, DeForest & Gurman (1998) report on quasi-periodic compressive waves in solar polar plumes which Ofman et al. (1999) consider to be slow magneto-acoustic waves. More recently, Aschwanden et al. (1999) reported the first detection of spatial displacement oscillations of coronal loops, observed for the first time due to the high spatial resolution of TRACE (Transition Region and Coronal Explorer). Nakariakov et al. (1999) analysed the transverse loop oscillations induced by a flare observed with TRACE and estimated that the coronal dissipation coefficient could be as much as eight or nine orders of magnitude larger than the theoretically predicted classical value. De Moortel et al. (2000a) report on the detection of propagating oscillations as observed in 171 Å by TRACE which they suggest to be propagating slow magneto-acoustic waves. Using a wavelet analysis, these authors found periods in the 200–400 seconds range.

In most cases these wave motions are not steady harmonic waves but tend to be waves with only a few periods and either are of finite lifetime or are damped. Therefore, Fourier analysis is not really appropriate as it is unable to provide any information about the lifetime of the oscillations and can only indicate the dominant frequencies (or wavelengths) present. Wavelet analysis is an important extension of Fourier analysis as it provides the time localisation of the frequency components. It is a powerful technique which allows a local decomposition of timescales in the time series. This makes the wavelet analysis ideal for analysing non-stationary time series or time series

Send offprint requests to: I. De Moortel (ineke@mcs.st-and.ac.uk)

where one expects localised variations of power. This analysing technique is used in many fields of physics that involve the study of (non-stationary) time series: e.g. acoustic, geophysics and helioseismology. Wavelet analysis has been used previously for analysing solar time series data; Vigouroux & Delache (1993) make a comparison between Fourier and wavelet analysis of the solar diameter variability. Aschwanden et al. (1998) used wavelets to examine power law like behaviour in time series of hard X-ray solar flares, Frick et al. (1997) analysed the variability of the solar cycle in time while Bocchialini & Baudin (1994) examine the frequency and duration of chromospheric quiet Sun velocity oscillations. Komm (1994) applied a wavelet analysis to magnetograms of quiet and active Sun. More recently, Mészárosová et al. (1999) did a Fourier and wavelet analysis of type 42SER and 41F solar radio burst for which they found dominant periodicities in the 40-3 s interval. Gallagher et al. (1999) used a wavelet analysis to show an apparent periodicity in pulse-like transient brightenings in the Quiet Sun network and the presence of a 3-minute oscillatory pattern in the intra-network regions, both in the chromospheric He I and the transition region O V lines. Ireland et al. (1999a) used wavelets to look for wave packets in active region CDS observations and Ireland et al. (1999b) analysed coronal heating events in high cadence TRACE data.

In this paper we investigate how a wavelet analysis can be used to find out more about the coronal plasma through which observed wave-like oscillations are propagating. The key point is that a detailed use of wavelet transforms can provide valuable diagnostic information through coronal seismology. We base this study on the results of De Moortel et al. (1999, 2000b). These authors studied phase mixing of Alfvén in a stratified and radially diverging, open atmosphere was studied in detail. Although slow magneto-acoustic waves seem to be observed more frequently, an example of a flare excited transverse wave has been observed (Nakariakov et al., 1999). Theoretical details of propagation of Alfvén waves are easily expressed analytically and many of their properties should transfer to slow waves propagating along magnetic field lines. A brief introduction to wavelet analysis and more details on some basic properties are described in Sect. 2. Sect. 3 considers the signature of finite wave trains, wave dissipation, gravitational stratification and a diverging atmosphere on the wavelet transform. Sect. 4 contains the discussion and conclussions.

2. Wavelet transform

In this section, we will give an overview of the method of wavelet analysis but for further details we refer the reader to Farge (1992) and Torrence & Compo (1998).

The continuous wavelet transform of a function $f(t)$ is defined as the convolution of $f(t)$ with an analysing function $\psi(\eta)$. To be called a wavelet, the analysing function must be localised both in time and frequency space and should be admissible, which, for an integrable function, means that its average should be zero (Farge 1992). We also assume that ψ is normalised, i.e. $\int_{-\infty}^{\infty} \psi\psi^* d\eta = 1$, where ψ^* is the complex conjugate. For $\eta = (t' - t)/s$ we have

$$W(t,s) = \int_{-\infty}^{\infty} f(t') \frac{1}{\sqrt{s}} \quad \psi^* \left[\frac{(t'-t)}{s} \right] dt' \,, \tag{1}$$

where t is time and s is the wavelet scale. The factor $\frac{1}{\sqrt{s}}$ is necessary to satisfy the normalisation condition taken as

$$\int_{-\infty}^{\infty} \psi \left[\frac{(t'-t)}{s} \right] \psi^* \left[\frac{(t'-t)}{s} \right] dt' = s \,.$$

For a discrete time series x_n of N observations with sample interval δt, the continuous wavelet transform is given by

$$W_n(s) = \sum_{n'=0}^{N-1} x_{n'} \sqrt{\frac{\delta t}{s}} \psi^* \left[\frac{(n'-n)\delta t}{s} \right] \,, \tag{2}$$

where s is the wavelet scale and n allows us to translate the analysing wavelet in time. In this case, the factor $\sqrt{\frac{\delta t}{s}}$ ensures that the normalisation condition is satisfied. The wavelet transforms at each scale s are now directly comparable to each other and to transforms of other time series. By varying s and n, one can build up a picture of any features in the time series as a function of the scale s and the localised time index n.

If a Fourier transform is taken of the data, so that

$$\hat{x}_k = \frac{1}{N} \sum_{n=0}^{N-1} x_n e^{-2\pi i k n/N} \,, \tag{3}$$

where $k = 0 \ldots N-1$ is the frequency index, then the wavelet transform can also be written as,

$$W_n(s) = \sum_{k=0}^{N-1} \hat{x}_k \sqrt{\frac{2\pi s}{\delta t}} \hat{\psi}^*(s\omega_k) e^{i\omega_k n \delta t} \tag{4}$$

where $\hat{\psi}$ is the Fourier transform of the function ψ and where the angular frequency is defined as

$$\omega_k = \begin{cases} \frac{2\pi k}{N\delta t} & \text{if } k \leq \frac{N}{2} \\ -\frac{2\pi k}{N\delta t} & \text{if } k > \frac{N}{2} \,. \end{cases} \tag{5}$$

Using Eq. (4) and a standard Fast Fourier Transform (FFT) routine, the continuous wavelet transform for a given s can be calculated at all n simultaneously. The wavelet power spectrum is defined as $|W_n(s)|^2$. Ranging through s and n will build up a two-dimensional time-frequency transform of the original time series. As the Fourier transform in Eq. (4) assumes the data is periodic, 'wrap-around' errors will occur at both edges of the transform when one is dealing with time series of finite length. One possible solution to this problem is to pad the end of the time series with zeroes before doing the wavelet transform. Unless otherwise stated, all solutions in this paper are obtained using a numerical code, based on Eq. (4), as it is numerically considerably faster to do the calculations for all n simultaneously in Fourier space. Whenever analytical approximations are calculated, they are based on Eq. (2).

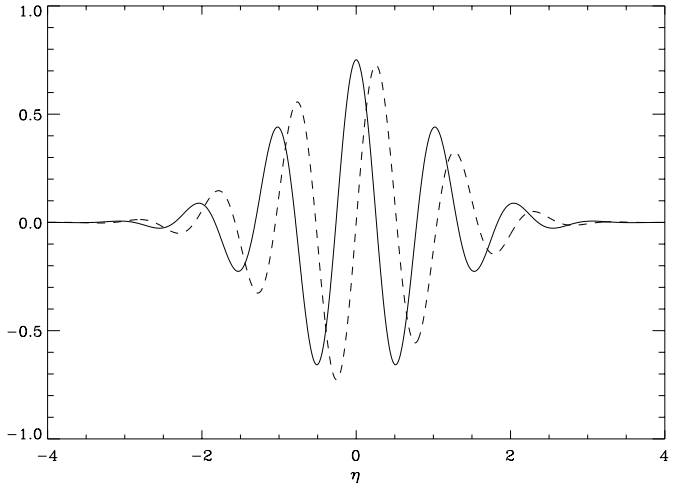

Fig. 1. Real (solid line) and imaginary (dashed line) part of the Morlet wavelet with $k = 6$.

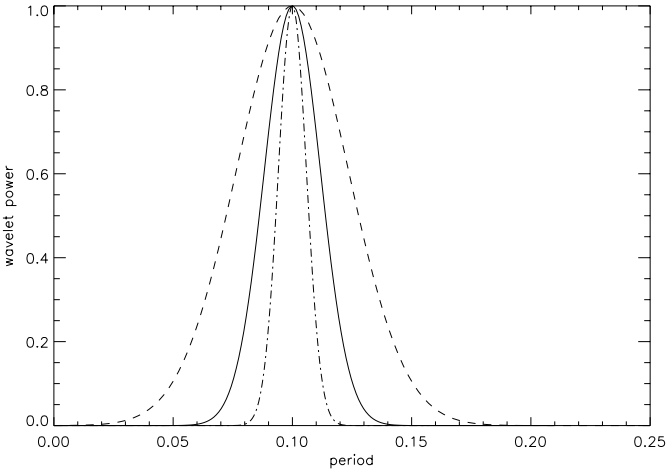

Fig. 2. Wavelet power for $f(t) = \cos lt$ with $l = 2\pi 10$ for different values of k; $k = 3$ (dashed line), $k = 6$ (solid line), $k = 12$ (dot-dashed line).

The choice of the appropriate analysis (or mother) wavelet depends on the nature of the signal and on the kind of information we want to extract from the signal. In this paper, we will use the (complex-valued) Morlet wavelet,

$$\psi(\eta) = \pi^{-1/4} \exp(ik\eta) \exp\left(-\frac{\eta^2}{2}\right) , \tag{6}$$

consisting of a plane wave modulated by a Gaussian, as our mother wavelet (Fig. 1). The Fourier transform of ψ is given by

$$\hat{\psi}(s\omega) = \pi^{-1/4} H(\omega) \exp\left(-(s\omega - k)^2/2\right) , \tag{7}$$

with $H(\omega)$ the Heaviside step function, $H(\omega) = 1$ if $\omega > 0$ and $H(\omega) = 0$ otherwise.

Now we have chosen a mother wavelet, we need to choose a set of scales s to use in the wavelet transform. Following Torrence & Compo (1998), we take

$$s_j = s_0 2^{j\delta j}, \qquad j = 0, 1, \ldots, J \tag{8}$$

where,

$$J = \delta j^{-1} \log_2(N\delta t/s_0) . \tag{9}$$

Here $s_0 = 2\delta t$ is the smallest scale and J determines the largest scale. The value of δj is chosen to be 0.125.

Because we work with finite time series, the wavelet transform suffers from edge effects at both ends of the time series, which results in a *cone of influence* (COI) in the transform. The cone of influence represents a measure of where the edge of the finite sample data has affected the analysis. As in Torrence & Compo (1998), the COI is defined so that the wavelet power for a discontinuity at the edges decreases by a factor e^{-2}. Portions of the transform that are outside the area formed by the 'time' axis and the cone of influence are subject to these edge effects and are therefore unreliable. The edge effects are more pronounced at larger scales as the influence of each wavelet extends further in time and larger parts of the discontinuities will enter the analysis. Overall, errors in the transform near the edges will be a combination of edge effects and the wrap-around of the Fourier transform.

2.1. Basic properties

In this section, we try to get a deeper understanding of the wavelet analysis and its basic properties, such as its time and scale resolution. Therefore, we calculate the wavelet transform of some basic and simple functions analytically. This will tell us how the value of the parameter k in Eq. (6) affects the resolution of the transform, which will help us chosing an appropriate value for k. We start by working out the wavelet power spectrum $|W|^2$ for the harmonic wave $f(t) = \cos lt$.

$$\begin{aligned} W(t,s) \;=\; & \frac{\pi^{-1/4}}{\sqrt{s}} \frac{1}{2} \int_{-\infty}^{\infty} (e^{ilt'} + e^{-ilt'}) \\ & \times e^{-ik\frac{(t'-t)}{s}} e^{-\frac{(t'-t)^2}{2\,s^2}} dt' . \end{aligned} \tag{10}$$

Setting $\eta = \frac{t'-t}{s}$, it is straightforward to calculate that the wavelet power is given by

$$\begin{aligned} |W|^2 \;=\; & \pi^{1/2} \frac{s}{2} \left[e^{-(ls-k)^2} + e^{-(ls+k)^2} \right. \\ & \left. + \cos 2lt \quad e^{-l^2 s^2 - k^2} \right] \\ \approx\; & \pi^{1/2} \frac{s}{2} \quad e^{-(ls-k)^2} . \end{aligned} \tag{11}$$

For positive scales, this function has a maximum at $s = \frac{k+\sqrt{k^2+2}}{2l}$. The period will then be given by

$$P = \frac{2\pi}{l} = Fs , \tag{12}$$

with $F = \frac{4\pi}{k+\sqrt{k^2+2}}$. So to extract the period of the signal from the wavelet analysis, we have to multiply the scales used in the analysis by this factor F. From this result, we also see that we will get a better scale (or frequency) resolution for larger values of k as the wavelet power behaves like a Gaussian function, centered around $s = \frac{k}{l}$. As illustrated in Fig. 2, the Gaussian gets narrower for larger values of k which will results in a more accurate resolution of the period. As k gets smaller, the Gaussian curve becomes wider which implies a loss of scale resolution.

As stated above, the analysing function must have zero mean to be admissible as a wavelet (Farge 1992). The Morlet wavelet is only marginally admissible, meaning that its average is never exactly zero. However, for $k = 6$, the average is of the order of 10^{-16} or smaller. For larger values of k, the scale resolution is improved (as illustrated in Fig. 2) but at the same time, temporal resolution is lost, which is why we choose the smallest value for k that makes the function admissible. So, from now on, we will set $k = 6$ in the Morlet wavelet (Eq. 6).

To illustrate this loss of temporal resolution analytically, we work out the wavelet power of the finite function $f(t) = \cos(lt)$ for $0 \leq t \leq a$ and $f(t) = 0$ elsewhere,

$$W(t,s) = \frac{\pi^{-1/4}}{\sqrt{s}}\frac{1}{2}\int_0^a (e^{ilt'} + e^{-ilt'}) \times e^{-ik\frac{(t'-t)}{s}} e^{-\frac{(t'-t)^2}{2\,s^2}}\,dt' \,. \quad (13)$$

Again setting $\eta = \frac{t'-t}{s}$, we find

$$W(t,s) = \sqrt{s}(\cos lt + i\sin lt)e^{-(ls-k)^2/2}\frac{\sqrt{2}}{\pi^{3/4}} \times \left[\mathrm{erf}\left(-i\frac{ls-k}{\sqrt{2}} + \frac{a-t}{\sqrt{2}s}\right) - \mathrm{erf}\left(-i\frac{ls-k}{\sqrt{2}} - \frac{t}{\sqrt{2}s}\right)\right],$$

where $\mathrm{erf}(x)$ is the Error function (Abramowitz & Stegun, 1965). As we are interested in the effect the value of k has on the temporal resolution of the maximum of the wavelet power, we set $s \approx \frac{k}{l}$. The wavelet power is then given by,

$$|W|^2 = \frac{k}{l}\frac{2}{\pi^{3/2}}\left[\mathrm{erf}\left(l\frac{a-t}{\sqrt{2}k}\right) + \mathrm{erf}\left(\frac{lt}{\sqrt{2}k}\right)\right]^2 . \quad (14)$$

In Fig. 3, we have plotted the wavelet power for the function $f(t) = \cos(lt)$ for $0 \leq t \leq a$ and $f(t) = 0$ elsewhere, for different values of k. We see that as k gets smaller, the Error function gets narrower which implies that the time resolution is improved. For larger values of k, the Error function becomes more and more spread out and the estimated time can be wrong with a factor of 2 or more. We also note that the loss of temporal resolution for larger k is stronger for smaller values of a.

3. Wavelet analysis of phase mixed Alfvén waves

Till now, we have analysed the wavelet transforms of a time series $f(t)$. However, it is also possible to take the wavelet transform of functions depending on spatial variables, rather than time. All results with respect to time and frequency resolution still apply and can now be though of as space and wavelength resolution. Using a wavelet analysis on phase mixed Alfvén waves, we now demonstrate that there is a distinct signature of phase mixing in the wavelet transform. Using this signature, it is possible to extract information from the wavelet transform about the physical surroundings in which the waves are propagating. Phase mixing in a stratified and radially diverging, open atmosphere was studied in detail by De Moortel et al. (1999, 2000b).

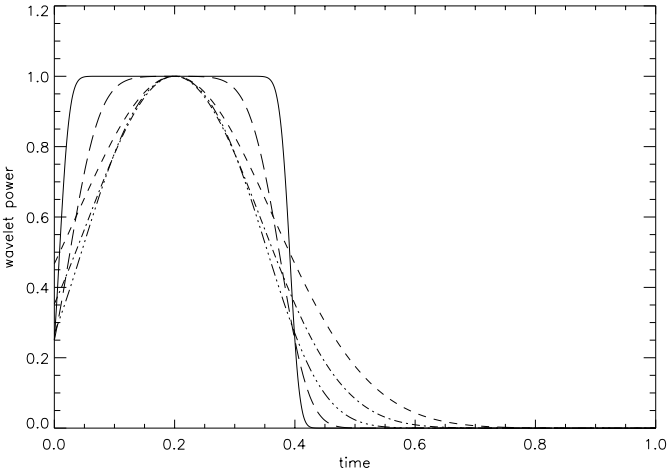

Fig. 3. Normalised wavelet power for $f(t) = \cos lt$ for $0 \leq t \leq a$ and $f(t) = 0$ elsewhere with $a = 0.4$, with $l = 2\pi 10$ for different values of k; $k = 1$ (solid line), $k = 3$ (long dashed line), $k = 6$ (dot-dot-dashed line), $k = 9$ (dot-dashed line), $k = 12$ (dashed line).

The effect of dissipation, stratification and divergence on phase mixing of Alfvén waves was described using both numerical and WKB solutions. In this paper we will use the approximate WKB solutions for phase mixed Alfvén waves in a diverging and gravitationally stratified atmosphere. For more details and for the derivation of these solutions, we refer the reader to De Moortel et al. (1999, 2000b). What is important here is not that we are analysing Alfvén waves as such but to show how wavelet analysis can provide valuable information about the coronal plasma. Slow and fast MHD waves will exhibit similar characteristics but cannot be treated in such a simple, analytical manner.

Including viscosity, the WKB solution for the perturbed velocity $\mathbf{v}$, in spherical (dimensionless) coordinates, is given by

$$v \approx \exp\left(-i\frac{2\pi r_0}{\lambda_0}K(\theta)R\right)\exp\left[\frac{1}{4H}\left(1-\frac{1}{r}\right) - \frac{1}{2}\Lambda_\nu^2\Omega\left(\frac{2\pi r_0}{\lambda_0}\right)^3 K(\theta)\int_1^r \times\left(\theta_0^2 r^6 e^{-\frac{1}{2H}\left(1-\frac{1}{r}\right)} + \frac{K'(\theta)^2}{K(\theta)^2}R^2 e^{\frac{1}{2H}\left(1-\frac{1}{r}\right)}\right)dr\right], \quad (15)$$

with $R = \int_1^r r^2 e^{-\frac{1}{2H}\left(1-\frac{1}{r}\right)}dr$ and the dissipation coefficient $\Lambda_\nu^2 = \frac{\rho_0\nu\Omega_0\mu}{B_0^2}\left(\frac{\lambda_0}{2\pi r_0\theta_0}\right)^2$ and where, for example, $K(\theta) = (1+\delta\cos(m\pi\theta))^{-1/2}$. The parameter δ regulates the magnitude of the equilibrium density variation, which causes phase mixing to occur. The radial distance r and the pressure scale height H are measured in units of the solar radius r_0. All the results described in this paper are obtained with $\delta = 0.5$. If one wants to study each physical effect separatly, gravitational stratification can be eliminated by setting the pressure scale height to infinity, i.e. $1/H = 0$. The spherical geometry allows the effect of flux tube divergence to be studied. If necessary, at low heights, i.e. $r \approx 1$

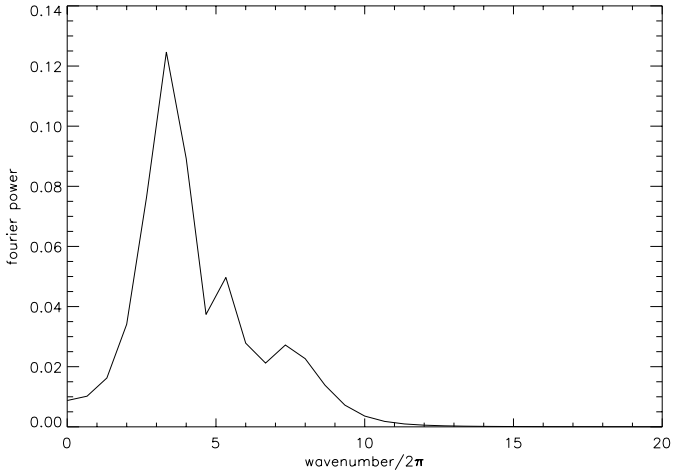

Fig. 4. Fast Fourier transform of the perturbed velocity at $x = 0.5$ in a stratified, non-dissipative plasma, with the pressure scale height $H = 0.5$ solar radii.

and for small initial wavelengths λ_0 the non-diverging Cartesian case can be retrieved by setting

$$r = 1 + \frac{\lambda_0}{2\pi r_0} z \qquad \text{and} \qquad x = r\theta\,. \tag{16}$$

The Cartesian coordinates have been made dimensionless by setting $x_0 = r_0\theta_0$ and $z_0 = \lambda_0/2\pi$ where λ_0 is the initial wavelength. We will calculate the WKB solution between $r = 1$ and $r = r_{max}$ in solar radii, or in Cartesian coordinates, between $z = 0$ and $z = z_{max}$ and θ (or x) between 0 and 1. As we are mainly interested in the behaviour of the waves as they propagate up in height, we will be looking at cross sections of the wavefront at $\theta = 0.5$ or, in Cartesian coordinates, $x = 0.5$.

Gravitational stratification was found to generate longer wavelengths and therefore phase mixing is less efficient and heat is deposited into the plasma at higher heights compared to a purely diverging atmosphere without stratification. At the same time the divergence results in shorter wavelengths which enhances phase mixing and heat is deposited at lower heights compared to a non-diverging atmosphere. So, compared to the original, uniform and unstratified Heyvaerts & Priest (1983) solution, phase mixing can be more or less efficient depending on the value of the scale height H. Finally, as an example we show the Fourier transform of a phase mixed Alfvén wave in a gravitationally stratified atmosphere in Fig. 4 (for the original signal, see Fig. 9). It is clear that the Fourier transform is not able to tell us anything about the basic wavelength or about the way the wavelength changes as the wave propagates up with heigth. It will become clear in the next sections that a wavelet analysis can provide a lot more information.

3.1. Finite wave trains

Considering the wavelet transform of a phase mixed wave in a uniform and unstratified plasma, i.e. with no gravitational stratification or radially divergence, as studied by Heyvaerts & Priest (1983). As the wave propagates up in height, dissipating by phase mixing will occur and the amplitude of wave will decrease to zero and the signal can thus be thought of as a finite wave. The perturbed velocity can be obtained from Eq. (15) by taking the Cartesian limit and setting $1/H = 0$ and is given by

$$v \approx \exp(-iK(x)z)\exp\left(-\frac{\Lambda_\nu^2}{6}\frac{K'(x)^2}{K(x)}z^3\right)\,, \tag{17}$$

The wavelet power is calculated by working out the integral

$$W(t,s) = \frac{\pi^{-1/4}}{\sqrt{s}}\int_0^{z_{max}} e^{-iK(x)z'}e^{-\varepsilon z'^3}e^{-ik\frac{(z'-z)}{s}} \times e^{-\frac{(z'-z)^2}{2\,s^2}}dz'\,, \tag{18}$$

where $\varepsilon = \frac{\Lambda_\nu^2}{6}\frac{K'(x)^2}{K(x)}$ and z_{max} is the upper boundary of the computational or observational window. The wavelet power will reach its maximum at $s_{max} \approx \frac{k}{K(x)}$ and is approximately given by

$$|W|^2 \approx \frac{k}{K(x)}\frac{4}{\pi^{3/2}}e^{-2\varepsilon z^3}\left[\text{erf}\left(\frac{(z_{max}-z)K(x)}{\sqrt{2}k}\right) + \text{erf}\left(\frac{zK(x)}{\sqrt{2}k}\right)\right]^2\,, \tag{19}$$

where $k = 6$. We want to compare these damped waves with a truly finite wave, i.e. a harmonic oscillation with the same wavelength $\lambda = 0.1$, that is cut off after a certain height. If there are distinct signatures in the wavelet transform that tell us the difference between both 'finite' signals, it might be possible to find out more about the involved dissipation mechanism when finite wave-like perturbations are observed.

Fig. 5 show the two finite signals we will be comparing. The harmonic signal in Fig. 5a is cut off after a height $1.75R_o$ while the signal in Fig. 5b is dissipated by phase mixing, i.e. by setting the dissipation coefficient $\Lambda_\nu^2 = 10^{-4}$ in Eq. (17) and taking a cross-section at $x = 0.5$. We now investigate whether the wavelet transform can indicate the difference between these two different signals.

The wavelet transform of the two different finite signals is displayed in Fig. 6. Both transforms indicate that an oscillation with a wavelength $\lambda = 0.1$ is present in the lower half of the region. As expected, we see that the wavelet power in the case of the damped wave (Fig. 6b) decreases more gradually than in the case of the finite harmonic wave (Fig. 6a).

But although there is some difference between the respective transforms, this difference is much clearer in Fig. 7. Here we plot a cross-section of the wavelet transform as a function of height, at its maximum power, i.e. at a wavelength $\lambda = 0.1$. The wavelet power in these figures has been normalised with respect to its maximum value. The power in Fig. 7a drops steeply to zero once the signal is cut off, while the power in Fig. 7b decreases more gradually as the amplitude of the signal is damped. Using the wavelet transform, it is possible to distinguish between a signal that switches off suddenly and a signal that is damped more gradually. Additionally, the steepness of the slope of the tranform in Fig. 7b indicates how strongly the wave is damped.

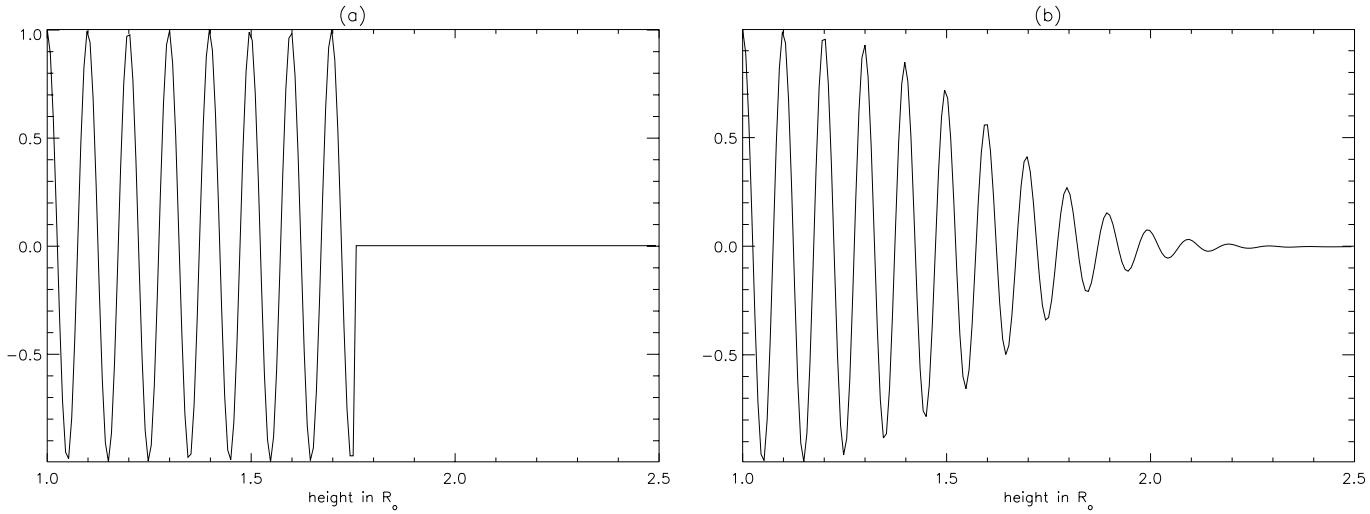

Fig. 5. a A harmonic oscillation with basic wavelength $\lambda = 0.1$, cut off after a height $1.75R_o$. **b** A cross-section at $x = 0.5$ of the perturbed velocity, calculated from Eq. (17), with the dissipation coefficient $\Lambda_\nu^2 = 10^{-4}$.

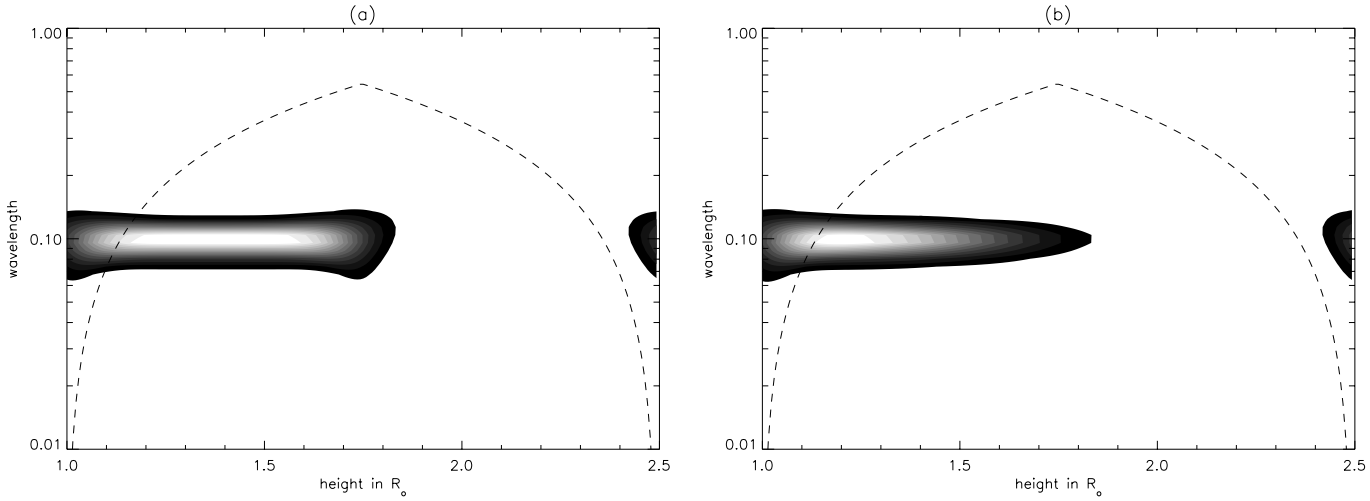

Fig. 6a and b. Corresponding wavelet transforms of the signals displayed in Fig. 5. The dashed lines indicate the cone of influence.

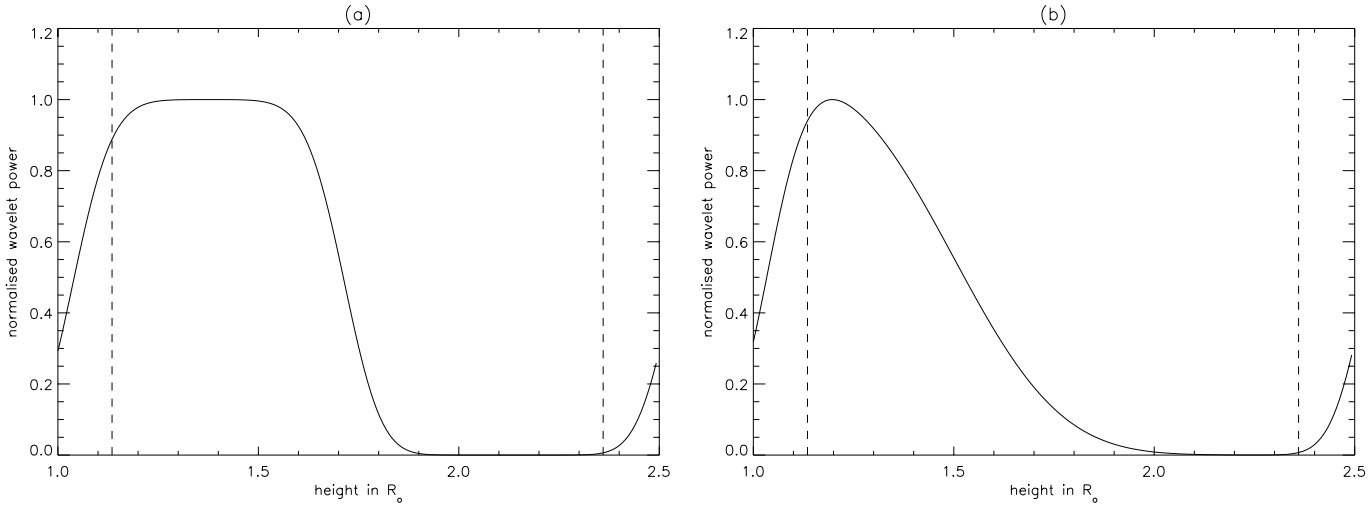

Fig. 7a and b. Cross-section of the (normalised) wavelet power at maximum wavelet power, i.e. at $\lambda = 0.1$ for **a** the finite harmonic wave and **b** for the phase mixed Alfvén wave. The dashed lines indicate the cone of influence.

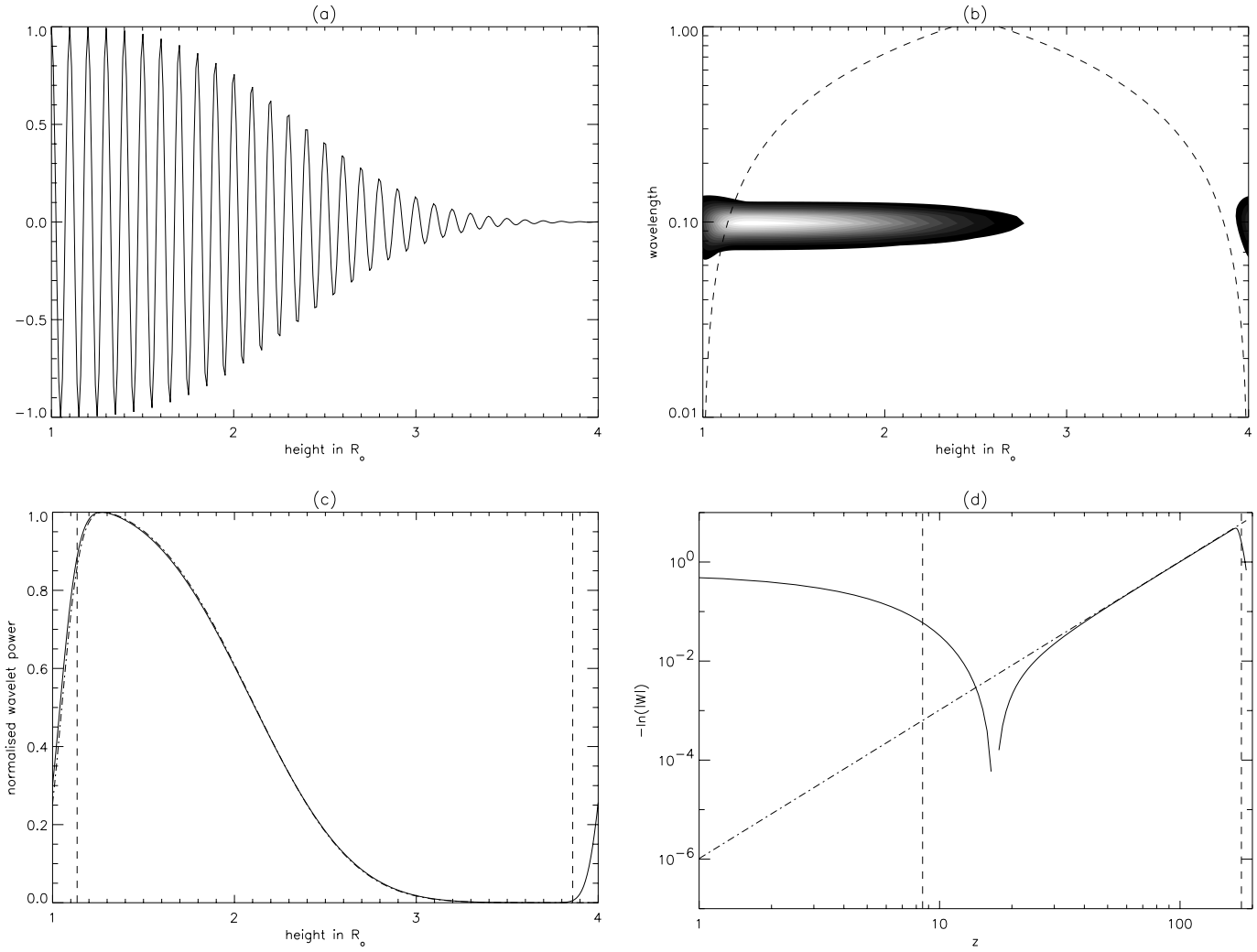

Fig. 8. a A cross-section at $x = 0.5$ of the perturbed velocity in a stratified, non-dissipative plasma, with $\Lambda_\nu^2 = 10^{-5}$. **b** Corresponding wavelet transform of the velocity at $x = 0.5$. **c** Cross-section of the (normalised) wavelet power at maximum wavelet power, i.e. at $\lambda = 0.1$. The dot-dashed line corresponds to the analytical approximation with $\varepsilon = 10^{-6}$. **d** Logarithmic plot of the cross-section of the wavelet power as a function of the Cartesian height z. The relation between r, the height in solar radii R_o, and z is given by Eq. (16). The dot-dashed line corresponds to $\ln(\exp(\varepsilon z^3))$.The dashed lines indicate the cone of influence.

3.2. Wave dissipation

In the previous section we have seen it is possible to tell from the wavelet transform that a signal is dissipated. We now try to find out more about the involved dissipation mechanism, from the wavelet analysis. If we look carefully at Eq. (19), we see that the wavelet power is approximately damped as $-\varepsilon z^3$, just as the phase mixed wave. If we can fit this analytical expression to the wavelet transform of an observed signal, this might imply that the observed signal is dissipated by phase mixing which means there must be an inhomogeneity in the background density. It will then also be possible to extract the value of the dissipation coefficient from the slope of the cross-section at the basic wavelength of the wavelet transform. As the value of the coronal viscosity and resistivity are still not exactly known, an estimate of their value will have important implications for many suggested coronal heating mechanisms.

The phase mixed signal plotted in Fig. 8a is obtained by setting $\Lambda_\nu^2 = 10^{-5}$ in the WKB solution (Eq. (17)) and taking a cross-section at $x = 0.5$. As the waves propagate up with height, the basic wavelength stays constant but the amplitude of the oscillation is damped as phase mixing occurs. Both these properties are visible in the wavelet transform (Fig. 8b). At all heights, the wavelet power is situated at the basic wavelength $\lambda = 0.1$. At larger heights, we see that the amplitude of the transform decreases, consistent with the decreasing amplitude of the original signal. The slight increase at the right hand edge is a consequence of the wrap-around effect, caused by the Fourier transform. However, this increase occurs outside the COI and should therefore not be taken into account anyway. In Fig. 8 (c), we have plotted a cross-section of the wavelet power at a constant wavelength $\lambda = 0.1$. The solid line corresponds to the numerical solution for the wavelet transform, whereas the

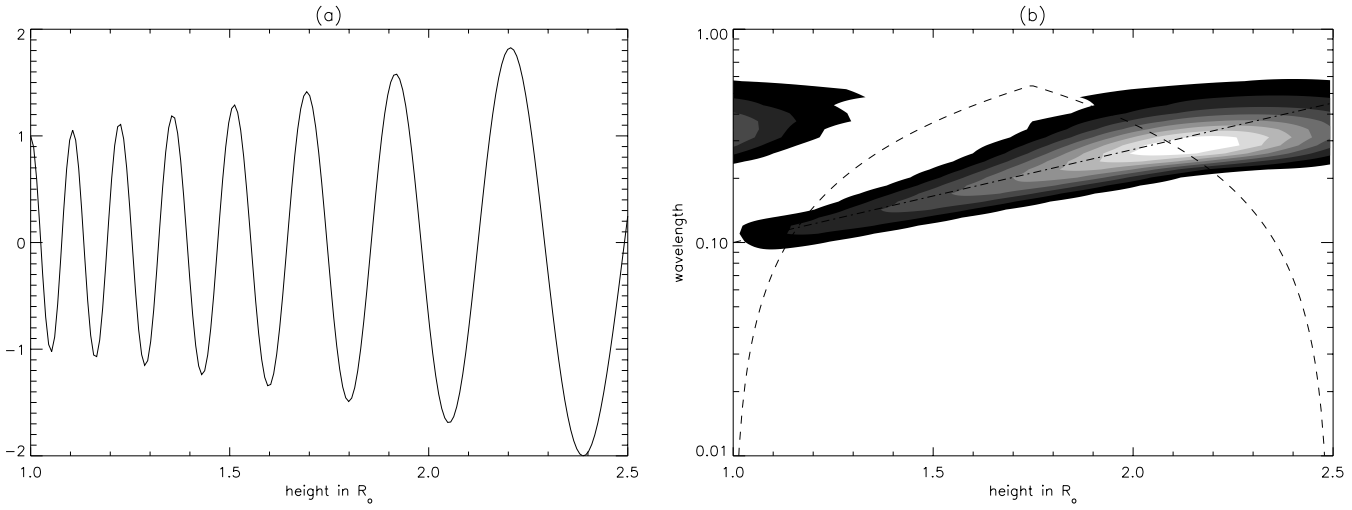

Fig. 9. a A cross-section at $x = 0.5$ of the perturbed velocity in a stratified,non-dissipative plasma, with the pressure scale height $H = 0.5$ solar radii. **b** Corresponding wavelet transform of the velocity at $x = 0.5$. The dot-dashed line represents $e^{z/2H}$. The dashed lines indicate the cone of influence.

dot-dashed line was obtained from the analytical approximation (Eq. (19)), setting $\varepsilon = 10^{-6}$. When comparing the expression for the dissipation coefficient Λ_ν^2, used in Eq. (17), with the expression for the parameter ε, used in Eq. (19), we see that $\Lambda_\nu^2 = 10^{-5}$ implies $\varepsilon \approx 10^{-6}$, at $x = 0.5$. The agreements between the numerical solution and the analytical expression is not bad. The difference near the edges is caused be the wrap-around error, coming from the Fourier transform that is used to obtain the numerical solution. The agreement at the edges can be improved by padding the signal with zeroes, before taking the wavelet transform. However, the $e^{-\varepsilon z^3}$ slope, which is a caracteristic signature of phase mixing, is clearly present in the transform. Additionally, the steepnes of this slope will give us an estimate for the value of the dissipative coefficient Λ_ν^2. Finally, Fig. 8d is a logarithmic version of Fig. 8c, plotted against the Cartesian height z (see Eq. (16)), rather than the height in R_o we have used so far. The dot-dashed line is simply $\ln(\exp(\varepsilon z^3))$, with $\varepsilon = 10^{-6}$. Inside the COI, the agreement between both solutions is remarkable and as $\ln(\exp(\varepsilon z^3)) = \varepsilon$ at $z = 1$, the value of the parameter ε is directly given by the intersection of εz^3 and the vertical axis. The gradient of the slope is three, corresponding to the power in the exponential damping due to phase mixing (see Eq. (17)). Alternative damping mechanisms would have a different slope in such a logarithmic plot.

From a wavelet analysis of this signal, we extracted a lot more information than just the wavelength(s) of the oscillations. The fact that $e^{-\varepsilon z^3}$ is an excellent fit implies that phase mixing is occuring, and hence, that there is a substantial density inhomogeneity present in the plasma. Furthermore, it is possible to estimate the value of the coronal dissipation coefficient from a logarithmic plot of the wavelet transform. It is important to note here that phase mixing is merely used as an example of a dissipation mechanism. Other dissipation mechanisms have their own characteristic damping profile, which will be present in the wavelet transfrom.

3.3. Gravitational stratification

In this section we neglect dissipation (by setting the dissipative coefficient $\Lambda_\nu^2 = 0$) and look at the effect of a gravitationally stratified atmosphere. We again use Cartesian coordinates. When a density inhomogeneity is present in both the horizontal and vertical direction, phase mixing will occur and as the phase mixed Alfvén waves propagate up with height, the amplitude of the perturbed velocity will increase as $\rho_0^{-1/4}$, due to the decreasing density ρ_0 (Wright & Garman, 1998; Torkelsson & Boynton 1998). Additionally, the wavelength λ will increase as $e^{z/2H}$, as the Alfvén speed v_A depends on height as $e^{z/2H}$, where H is the pressure scale height (De Moortel et al. 1999). For the results presented in this section, we set $H = 0.5$. Again, we want to find out if the wavelet transform indicates that gravitational stratification is present in the surroundings where oscillations are observed. Although the pressure scale height H can be calculated from temperature estimates, it would be nice to confirm this value from the wavelet transform.

In Fig. 9a, we plotted a cross-section of the perturbed velocity, again at $x = 0.5$. It is clear that both the amplitude and the wavelength increase as the wave propagates up with height. The wavelet transform (Fig. 9b) confirms that increasingly longer wavelengths are present with increasing height. The increasing amplitude of the wavelet transform is caused by a combination of the amplitude increase of the perturbed velocity and the lengthening of the wavelengths at larger heights. The fact that the transform starts decreasing again is purely caused by the wrap-around error of the Fourier transform. In this Fig. , we also plotted (dot-dashed line) $e^{z/2H}$ as a function of height, the wavelength variation we expect from previous studies. We see that, apart from outside the cone of influence, where edge effects become to large to trust the transform, the $e^{z/2H}$ variation of the wavelength is remarkably well represented in the wavelet power. So when an increase in wavelength

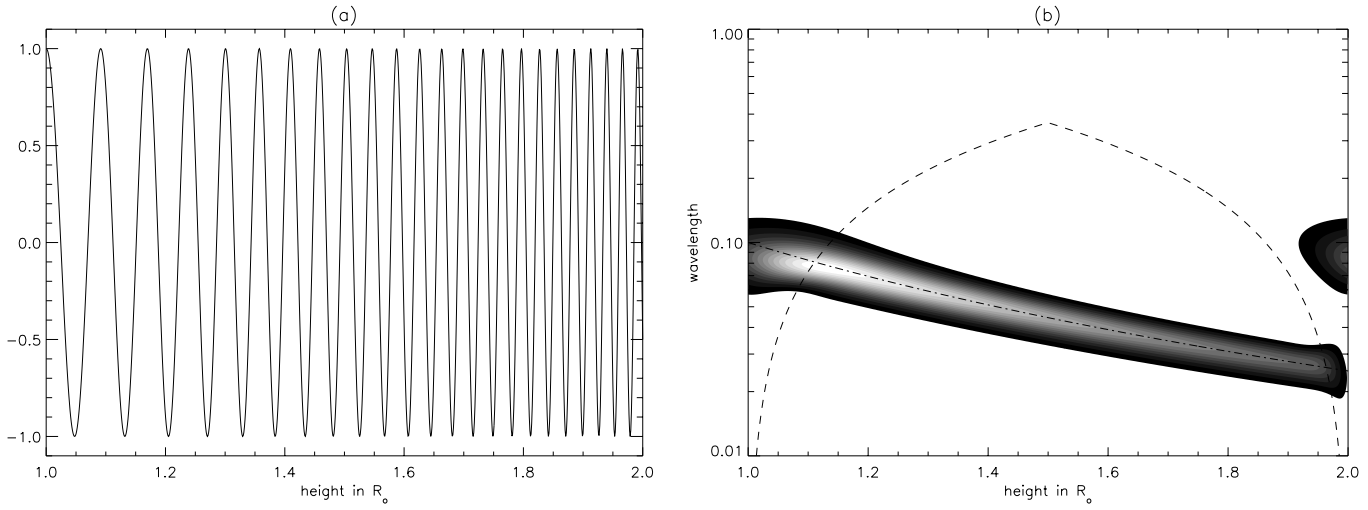

Fig. 10. a A cross-section at $\theta = 0.5$ of the perturbed velocity in a non-dissipative plasma, with a radially diverging background magnetic field **b** Corresponding wavelet transform of the velocity at $\theta = 0.5$. The dot-dashed line represents $\frac{1}{r^2}$. The dashed lines indicate the cone of influence.

is present in the wavelet transform of observed oscillations, the pressure scale height H can be obtained by fitting an $e^{z/2H}$ curve through the wavelet power. Unfortunately, as the wavelength increases when the waves propagate up with height, an increasingly larger portion of the transform will fall outside the COI. So for a strongly stratified atmosphere, i.e. for small values of the pressure scale height H, it might be difficult to fit the $e^{z/2H}$ curve to the transform. However, despite this, there clearly is a lot more information in the wavelet transform then there is in the Fourier transform of the same signal (Fig. 4).

3.4. Diverging atmosphere

Finally, we study the effect of a radially diverging background magnetic field. We exclude dissipation ($\Lambda_\nu^2 = 0$) and gravitational stratification ($H \rightarrow \infty$) from the model and work with spherical coordinates, as they will be the most convenient choice. As a density inhomogeneity is still present in the horizontal direction, phase mixing of Alfvén will again occur as the waves propagate up with height. De Moortel et al. (2000b) found that, unlike gravitational stratification which lengthens the wavelength, area divergence shortens the wavelength. Indeed, both the Alfvén speed and the wavelength λ will decrease as $\frac{1}{r^2}$. As the background density is independent of height, the amplitude of the perturbed velocity remains constant.

The cross-section of the perturbed velocity in Fig. 10a shows the constant amplitude and the rapidly decreasing wavelength with increasing height. As the wavelengths decrease continuously, it is important to include a sufficiently high number of scales in the wavelet analysis, to ensure that all wavelengths are fully resolved. Therefore, we decrease the value of δj, which determines the number of scales included in the wavelet analysis, to 0.025 in this section. The wavelet transform (Fig. 10b) confirms the decreasing wavelength as wavelet power is present at continuously smaller wavelengths for larger heights. The dot-dashed line overplotted is the expected wavelength change $\frac{1}{r^2}$. Just as in the gravitational stratification case, the wavelet transform follows the theoretically predicated change in wavelength extremely well, inside the cone of influence. As for smaller scales (or wavelengths in this case) larger portions of the transform fall inside the COI, the $\frac{1}{r^2}$ change in wavelength can be followed for almost the entire duration of the signal. When this $\frac{1}{r^2}$ curve fits the transform, and there is no (radial) change in the background density, this implies that the backround magnetic field is radially diverging.

4. Discussion and conclusions

In this paper we applied a wavelet analysis to phase mixed Alfvén waves in various physical circumstances. We briefly introduced the wavelet analysis and then discussed its resolution properties in more detail. In a first stage we compared two finite signals, dissappearing at a similar height. The first one being a simple harmonic wave, cut off at this height, and the second one being an Alfvén wave, dissipated by phase mixing. Apart from indicating the wavelength present in the signals, the wavelet transform is distinctly different for a truly finite oscillation and for a gradually damped oscillation. Thus, when observing oscillations fo finite lifetime, one can use a wavelet analysis to determine whether the signal is simply cut off, or gradually dissipated. Additionally, it is possible to have an estimate for the value of the dissipation coefficient by fitting an analytical approximation to the numerical solution for the wavelet transform. As the εz^3 slope of the analytical fit is a typical characteristic of phase mixing, a good fit between this approximation and the transform of the analysed signal could imply that the signal is dissipated by phase mixing. Other dissipation mechanisms will have their own characteristic slope, which will be evident in the wavelet transform. When applying these results to observational data, this could supply us with information on which dissipation is involved in the damping of the observed oscillation. The same method was followed in studying phase mixing of Alfvén waves

in a gravitationally stratified or a radially diverging atmosphere. The $e^{z/2H}$ lengthening of the wavelengths that occurs when Alfvén waves propagate through a vertically stratified plasma, is clearly evident in the wavelet transform. From this a value for the pressure scale height can be estimated and, when possible, compared to values obtained by different methods, e.g. when the temperature of the surroundings is known. Similarly, the $\frac{1}{r^2}$ behaviour of the wavelength in an atmosphere with a radially diverging background magnetic field, is also present in a wavelet transform of such an oscillation. In general, the wavelength is given by $2\pi v_A/\omega$. Thus, the variation in wavelength with height, as given by the wavelet analysis, provides information about the coronal Alfvén speed. Hence, we have a measure of both the coronal density and the coronal magnetic field variation.

Although this first, purely theoretical study, considered the propagation of Alfvén waves in an inhomogeneous corona, because they can be described by a single WKB expression, it indicates that a wavelet analysis of oscillations can provide important information about the physical surroundings in which the oscillations are found. An obvious next step is to apply the methods and results presented in this paper to oscillations observed in the solar corona. Due to its high spatial and temporal resolution, TRACE data provide an excellent opportunity to investigate waves in the solar corona and, through a wavelet analysis, provide estimates for local coronal plasma properties. Although the spatial and temporal resolution of the present generation spacecrafts might not be sufficient to perform an analysis as detailed as the one described in this paper, it will be possible to obtain an estimate for some of the coronal parameters. Examples of the implications of the results we presented here on the analysis of observational data will be presented in De Moortel et al. (2001).

Acknowledgements. The authors would like to thank Drs. G. Compo, J. Ireland and R.W. Walsh for many useful discussions on wavelet analyis. Wavelet software was provided by C. Torrence and G. Compo, and is available at URL: http://paos.colorado.edu/research/wavelets. I. De Moortel is supported by E.U. grant ERBFMBICT982880.

References

Abramowitz, M., Stegun, I.A.: 1965, Handbook of mathematical functions, Dover
Aschwanden, M.J., Kliem, B., Schwarz, U., et al., 1998, ApJ 505, 941
Aschwanden, M.J., Fletcher, L., Schrijver, C.J., Alexander, D., 1999, ApJ 520, 880
Bocchialini, K., Baudin, F., 1994, A&A 299, 893
Browning, P.K., 1991, Plasma Phys. and Controlled Fusion 33, 539
DeForest, C.E., Gurman, J.B. 1998, ApJ 501, L217
De Moortel, I., Hood, A.W., Ireland, J., Arber, T.D., 1999, A&A 346, 641
De Moortel, I., Ireland, J., Walsh, R.W., 2000a, A&A 355, L23
De Moortel, I., Hood, A.W., Arber, T.D., 2000b, A&A 354, 334
De Moortel, I., Ireland, J., Walsh, R.W., Hood, A.W., 2001, *in preparation*
Farge, M., 1992, Annu. Rev. Fluid Mech. 24,395
Frick, P., Galyagin, D., Hoyt, D.V., Nesme-Ribes, E., Schatten, K.H., Sokoloff, D., Zakharov, V., 1997, A&A 328, 670
Gallagher, P.T., Phillips, K.J.H., Harra-Murnion, L.K., Baudin, F., Keenan, F.P., 1999, A&A 348, 251
Heyvaerts, J., Priest, E.R.,1983, A&A 117, 220
Ireland, J., 1996, Ann. Geophys. 14, 485
Ireland, J., Walsh, R.W., Harrison, R.A., Priest, E.R., 1999a, ESA-SP 446
Ireland, J., Wills-Davey, M., Walsh, R.W., 1999b, Solar Physics 190, 207
Komm. R.W., 1994, ASP Conference Series 68, 24
Mészárosová, H., Jiricka, K., Karlicky, M., 1999, A&A 348, 1005
Nakariakov, V.M., Ofman, L., DeLuca, E.E., Roberts, B., Davila, J.M., 1999, Science 285, 862
Narain, U., Ulmschneider, P., 1996, Space Sci. Rev. 75, 453
Ofman, L., Nakariakov, V.M., DeForest, C.E., 1999, ApJ 514, 441
Torkelsson, U., Boynton, G.C., 1998, MNRAS 295, 55
Torrence, C., Compo, G.P., 1998, Bull. Amer. Meteor. Soc. 79, 61
Vigouroux, A., Delache, Ph., 1993, A & A 278, 607
Wright, A.N., Garman, A.R., 1998, Journal of Geophysical Research 103, 2377
Zirker, J.B., 1993, Solar Physics 148, 43